The Aeronautical Journal (2025), **129**, pp. 3467–3483
doi:10.1017/aer.2025.10051

RESEARCH ARTICLE

A minimum selection strategy for control of small-scale turbojet engines

A. Imani

Department of Mechanical Engineering, Faculty of Engineering, Bu-Ali Sina University, Hamedan, Iran
Email: a.imani@basu.ac.ir

Received: 10 September 2024; **Revised:** 28 June 2025; **Accepted:** 2 July 2025

Keywords: minimum selection; saturation function; small turbojet engine; stability assurance; thermodynamic model

Abstract

Control of small turbojet engines is challenging due to the small number of sensors and actuators. In these engines, typically the spool speed and exhaust gas temperature are the measured variables and the fuel flow is the only manipulated variable. However, the thrust command must be achieved and the engine's structural and operational limitations must be safeguarded. In this research, a minimum selector control structure with a saturation function is presented for controlling small turbojet engines. One control loop is considered to control the spool speed and another loop is used to manage the exhaust gas temperature. The output of the control loops is the fuel flow rate and the minimum value is selected between them. To prevent the compressor surge and combustor blow-out during engine acceleration/deceleration, a fuel flow rate saturation is defined. Due to the switching structure of the proposed controller and existence of the saturation function, stability analysis is a critical issue. Therefore, a methodology is presented to analyse the stability of the proposed structure. In simulation study, a nonlinear thermodynamic model that matches more than 90% with the test data is used and the response of the proposed controller is compared with a proportional integral (PI) controller. In a comprehensive scenario, the throttle degree varies from 75% to 100%. Using the PI controller, some outputs have some overshoot and the exhaust gas temperature exceeds the corresponding constraint by 40K. While the proposed minimum selector controller, in addition to accurately fulfilling the thrust command, fully protects the limitations governing engine variables.

Nomenclature

a, b, c_i, d_i	model parameters
A, B, C_i	augmented model matrices
A_e	exit area
C_v	nozzle exit velocity coefficient
EGT	exhaust gas temperature
FAR	fuel to air ratio
G	transfer function
h	enthalpy
H	fuel heating value
I	identity matrix
ISA	International Standard Atmosphere
J	moment of inertia of the rotor
K	percentage of pressure drop
K_i	feedback gain i
$\dot{m}$	mass flow
M	Mach
N	spool speed
$\dot{N}$	spool acceleration

© The Author(s), 2025. Published by Cambridge University Press on behalf of Royal Aeronautical Society.

https://doi.org/10.1017/aer.2025.10051 Published online by Cambridge University Press

N_c	corrected spool speed
p_i	reference prefilter gain i
P_{amb}	ambient pressure
P_s	Sstatic pressure
P_{std}	standard pressure
P_{tin}	total inlet pressure
P_{tout}	total outlet pressure
PI	proportional integral controller
PLA	power level angle
r_i	setpoint i
SLS	standard sea-level
t_i	output of memory-less function i
T_{std}	standard temperature
T_{tin}	total inlet temperature
T_{tout}	total outlet temperature
u	control input
u_r	control input rate
V	Lyapunov function
W_f	fuel flow
x	state variable
X	augmented state vector
y_i	increment of the output i
z_i	input of memory-less function i

Greek symbol

δ	non-dimensional pressure
η	efficiency
θ	non-dimensional temperature
Λ	vector containing static nonlinearities
π	pressure ratio
τ	torque
Ω_i	diagonal matrix i for sector definition

1.0 Introduction

The application of small turbine engines for aircraft propulsion is remarkable. In this area, microjet engines are more preferred because of their straightforward design, fewer components, and lower cost. A significant challenge with these engines is the availability of limited sensors for control and condition monitoring. Typically, these engines are equipped with only two sensors: one for measuring engine speed, and another for exhaust gas temperature. On the other side, fuel flow is the sole variable used for managing thrust and operational limits. Despite these circumstances, these engines must exhibit efficient performance across a range of flight conditions, including varying Mach numbers and altitudes. To enhance the design and efficiency of small turbojet engines, numerous studies have been carried out focusing on modeling, performance analysis, and the development and implementation of control systems. In research conducted by Catana et al. [1], the primary parameters and performance assessment of microjet engines were examined during the take-off phase as well as under various operating conditions. The analysis was based on thermodynamic evaluations of several engines produced by various manufacturers, including JetCat and AMT Netherlands. The engines examined featured an identical spool design, yet they varied in thrust classes, with outputs ranging from 97 to 1569 N. In another study, Erario et al. [2] created a numerical model of a micro gas turbine designed to predict and assess engine performance using the gas turbine simulation program (GSP). To evaluate the engine's performance during bench and flight tests, they employed scaled maps of the compressor and turbine within a zero-dimensional model. The exhaust gas temperature (EGT) and fuel flow were selected as the primary parameters to validate

https://doi.org/10.1017/aer.2025.10051 Published online by Cambridge University Press

the model by comparing the numerically predicted values with the experimental data. Gaitanis et al. [3] introduced a numerical tool created using the Python programming language, aimed at predicting the performance of micro gas turbines. The primary objective of their research was to attain a high level of accuracy in the simulated dynamic responses. A significant advantage of this tool lies in its uncomplicated component modules. They validated their model through experimental data obtained from the VUB T100 test rig. In another research [4], a parametric white-box model was developed to capture the transient dynamics of the JetCAT P100-RX turbojet engine using MATLAB/Simulink. In this investigation, scaling techniques were employed to adjust the component performance maps. A state-space representation of the engine was established, and critical parameters were determined through system identification methods. In a separate study [5], researchers proposed a methodology for estimating online thrust for the small-scale turbojets utilised in aerial robots. They implemented a grey-box approach to model the dynamics of the turbojet system using a nonlinear state-space framework, informed by data collected from a specially designed engine test bench. This model subsequently facilitated the design of an extended Kalman filter, which estimates turbojet thrust based solely on angular speed measurements. In research by Metin and Aygun [6], dynamic energetic and performance measures of a small turbojet engine were calculated at various shaft speeds. Then, based on the calculated parameters, efficiencies, power and energy indexes of the engine were extracted. In another study by Aygun et al. [7], thrust, exhaust gas temperature and specific fuel consumption of a micro turbojet engine (MTJ-E) were predicted by a machine learning technique and using the experimental data of fuel flow, air mass flow, exhaust gas velocity, compressor inlet and outlet pressures and turbine RPM.

Several studies have been published regarding the control of small turbojet engines. Banazadeh et al. [8] employed an identification technique alongside frequency response test data to identify the transfer functions linking fuel flow to thrust, spool speed, compressor outlet pressure and turbine outlet temperature in a microturbine engine. Subsequently, they created a proportional integral derivative (PID) controller for the nonlinear system based on the models obtained. In a separate study, researchers introduced a modular control system for small gas turbine engines [9]. This control framework utilised situational control methodology and incorporated a diagnostic system as well. The controller was successfully implemented in a laboratory setting for the ISTC-21v and TJ-100 small turbojet engines. Beneda and Derbel [10] employed the turbofan power ratio, typically applied to high-bypass turbofan engines, to control a micro-turbojet engine. They developed a two-degree-of-freedom PID controller for the engine. In another research [11], they designed a sliding mode controller based on the turbofan power ratio. They modeled a small turbojet engine in the form of a linear parameter varying (LPV) structure and compared the performance of the proposed controller with a PID controller. Tang et al. [12] developed an adaptive PID controller based on neural networks for a micro-turbojet engine used in small unmanned aircraft. Their design allowed for real-time adjustment of the controller coefficients. While they applied their approach to control the engine spool speed, they did not consider the limitations associated with the engine's variables. Shehata et al. [13] provided a digital PID controller specifically for the JetCat-P200sx micro turbojet engine, employing an optimal control approach and a genetic algorithm to fine-tune the controller coefficients. They assessed the robustness of both methods by evaluating their effectiveness in noise and disturbance rejection. In a separate investigation, they utilised an adaptive fuzzy approach to modify the controller coefficients and examined the controller's performance in relation to the engine model within the MATLAB-Simulink environment [14]. Gao et al. [15] developed a PID controller to attain a stable control of engine speed during slow engine operating conditions. To optimise the tuning of the PID parameters, they proposed an enhanced evolutionary strategy for the self-adjustment of control variables within the engine speed and fuel flow management system. In another study [16], researchers examined the active disturbance rejection control (ADRC) approach to improve the disturbance resistance of the control system for a small-scale turbojet engine. They established an ADRC scheme with spool speed as the controlled variable and evaluated its performance against a PID control method through simulation experiments.

In most of the control methods developed for small turbojet engines in the open literature, traditional control techniques are employed to manage engine thrust. However, these control systems typically do

https://doi.org/10.1017/aer.2025.10051 Published online by Cambridge University Press

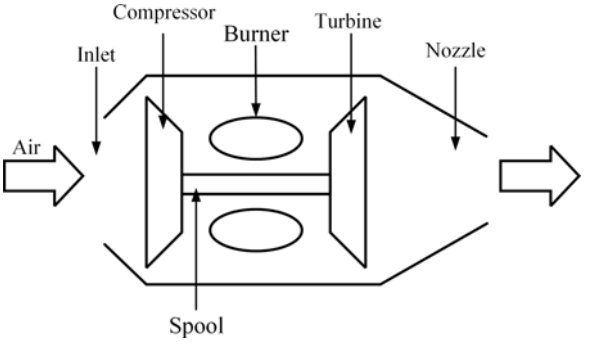


Figure 1. *Schematic of the studied turbojet engine.*

not incorporate critical engine constraints such as turbine temperature limits, compressor surge margin and combustor blow-out into their strategy. As a result, most of the proposed controllers lack the necessary depth and effectiveness for practical application. Therefore, utilising a decentralised architecture with multi-loop control systems for engine thrust control and limit management is more efficient than relying on a centralised structure. In this context, a Min-Max controller was developed for a turbojet engine by Jafari and Nikolaidis [17]. To enhance the controller's performance in terms of thrust tracking and response speed, fuzzy T and S norms were utilised instead of the conventional minimum and maximum functions. Their proposed scheme incorporated only proportional (P) controllers and did not take into account the turbine temperature limit. Furthermore, there was no strategy outlined for assessing the stability of the multi-loop system. Numerous studies [18–20] have explored the application of selector control schemes for managing large turbofan engines. Additionally, some research has introduced techniques to examine the stability of the control structure [21, 22]. However, microjet engines are equipped with significantly fewer sensors and actuators compared to large turbofan engines, which complicates the tasks of controlling engine thrust and ensuring limit protection. To date, no thorough methodology has been presented that utilises a selective control structure along with a stability analysis procedure for small turbojet engines which only involve two measured variables and a single manipulated variable.

In this paper, a control algorithm is presented for control of small turbojet engines that only have two measured variables, and only one control input. In this algorithm, state feedback regulators are used to control the thrust and turbine temperature. Fuel flow rate saturation is also used to control the compressor surge and combustion chamber blow-out. Due to the presence of the minimum selector and the saturation function in the proposed algorithm, the issue of system stability is very important, and in this research, an efficient method for analysing the stability is presented. In order to assess the effectiveness of the developed controller, a simulation study is carried out employing a non-linear thermodynamic model of a small turbojet engine.

2.0 Thermodynamic modeling of the engine

In the current research, the AMT NL Titan 40kg thrust engine is taken into account as a small-scale turbojet engine [23]. Figure 1 illustrates the primary structure of this engine, while its specifications are detailed in Table 1. The engine features a single-stage centrifugal compressor, an annular combustion chamber, and a single-stage axial turbine, and it is used as the propulsion system for some aerial vehicles such as the DEMON UAV [24].

The thermodynamic model of the engine developed in this study is based on a component-level framework. It is derived from the thermodynamic relations for the various engine components, including compressor, combustion chamber, turbine and nozzle. Additionally, it incorporates performance map data for the compressor and turbine [25, 26]. The average properties of the fluid at the input and output of each component are taken into account, and the scaled maps for the compressor and turbine are utilised. Engine modeling is conducted within the MATLAB-Simulink environment, and

https://doi.org/10.1017/aer.2025.10051 Published online by Cambridge University Press

Table 1. *Specifications of the studied engine [23]*

Parameter	Value
Thrust (N)	392
Engine rotational speed (RPM)	96,000
Inlet air mass flow (g/s)	660
Compressor pressure ratio	3.8
Exhaust gas temperature (C)	850
Fuel flow (g/s)	17
Specific fuel consumption (g/kN.s)	43.3

some of the capabilities of the toolbox for modeling and analysis of thermodynamic systems (T-MATS) offered by NASA Glenn Research Center (GRC) are utilised [27]. The relationships governing the engine components are described in the following subsections.

2.1 Compressor

Turbine engines are equipped with a compressor that increases the pressure of the incoming air before it reaches the combustor. The algebraic equations governing the compressor are described as follows [28]:

$$\begin{aligned}
\theta &= \frac{T_{tin}}{T_{std}}, \quad \delta = \frac{P_{tin}}{P_{std}}, \quad N_c = \frac{N}{\sqrt{\theta}} \\
\dot{m}_{c,map} &= f_1\left(N_c, \beta line\right) \\
\pi &= f_2\left(N_c, \beta line\right) \\
\eta &= f_3\left(N_c, \beta line\right) \\
\dot{m}_{out} &= \frac{\dot{m}_{c,map}}{\sqrt{\theta}\Big/\delta} \\
h_{tout} &= \frac{h_{tout,ideal} - h_{tin}}{\eta} + h_{tin} \\
P_{tout} &= \pi\left(P_{tin}\right), \quad T_{tout} = f\left(P_{tout}, h_{tout}\right) \\
\tau &= \frac{\dot{m}_{out}\left(h_{tin} - h_{tout}\right)}{N\left(\frac{2\pi}{60}\right)}
\end{aligned} \tag{1}$$

where f_1, f_2 and f_3 are functions or lookup tables that represent the compressor map. Gas properties such as enthalpy and temperature are determined using gas tables.

2.2 Combustion chamber

In the combustion chamber, injected fuel is combined with compressed air and after combustion, high temperature gas is produced. The hot gas drives the turbine and create thrust as it passes through the nozzle. The pressure drop in the combustion chamber is assumed to be constant. The relationships related to this component are expressed as follows:

$$\begin{aligned}
P_{tout} &= (1 - K)\, P_{tin} \\
\dot{m}_{gas,out} &= \dot{m}_{air,in} + \dot{m}_f \\
h_{tout} &= \frac{\eta_b \dot{m}_f H + \dot{m}_{in} h_{tin}}{\dot{m}_{out}} \\
FAR &= \frac{\dot{m}_f}{\dot{m}_{air,in}}
\end{aligned} \tag{2}$$

https://doi.org/10.1017/aer.2025.10051 Published online by Cambridge University Press

where $K = 0.05$ is the percentage of pressure drop in the combustor and H is the heating value of the fuel.

2.3 Turbine

Gas expansion in the turbine generates work of the rotor and drives the compressor. The turbine processes can be represented as follows:

$$\begin{aligned}
\theta = \frac{T_{tin}}{T_{std}}, \quad \delta = \frac{P_{tin}}{P_{std}}, \quad N_c = \frac{N}{\sqrt{\theta}} \\
\dot{m}_{out} = g_1\,(N_c, \beta line) \\
\pi = g_2\,(N_c, \beta line) \\
\eta = g_3\,(N_c, \beta line) \\
h_{tout_g} = h_{tin} - (h_{tin} - h_{tout_g,ideal})\eta \\
P_{tout} = \pi\,(P_{tin})\,, \quad T_{tout} = f\,(P_{tout}, h_{tout}) \\
h_{tout} = \frac{1}{\dot{m}_{out}}\left[h_{tin}\dot{m}_{tin} + \eta(h_{tin} - h_{tout_g,ideal})\dot{m}_{in}\right] \\
\tau = \frac{\dot{m}_{out}(h_{tin} - h_{tout_g})}{N\left(\frac{2\pi}{60}\right)}
\end{aligned} \tag{3}$$

similar to the compressor, g_1, g_2 and g_3 are a set of functions or lookup tables that define the turbine map.

2.4 Nozzle

The engine nozzle has a constant outlet area and is a converging type. In addition to the characteristics of the fluid entering the nozzle, the ambient static pressure at the nozzle exit affects the nozzle flow. Flow characteristics according to choking and non-choking conditions of the flow are specified by comparing the nozzle pressure ratio to the critical pressure.

$$\begin{aligned}
\pi = \frac{P_{tin}}{P_{amb}} \\
P_s = g(h_{tin}, P_{tout}, M = 1) \\
\pi_{critical} = \frac{P_{tin}}{P_s} \\
\text{If } \pi > \pi_{critical} \\
[P_s, u] = g_1(h_{tin}, P_{tout}, M = 1) \\
\text{else} \\
[P_s, u] = g_2(h_{tin}, P_{tout}, P_s = P_{amb}) \\
Thrust = \dot{m}_{out}uC_v + (P_{out} - P_{amb})A_e, \quad C_v = 1
\end{aligned} \tag{4}$$

2.5 Shaft

Using the torque supplied by the turbine and the torque used by the compressor, the shaft dynamics can be written as follows:

$$\dot{N} = \frac{\Delta\tau}{J\left(\frac{2\pi}{60}\right)} \tag{5}$$

https://doi.org/10.1017/aer.2025.10051 Published online by Cambridge University Press

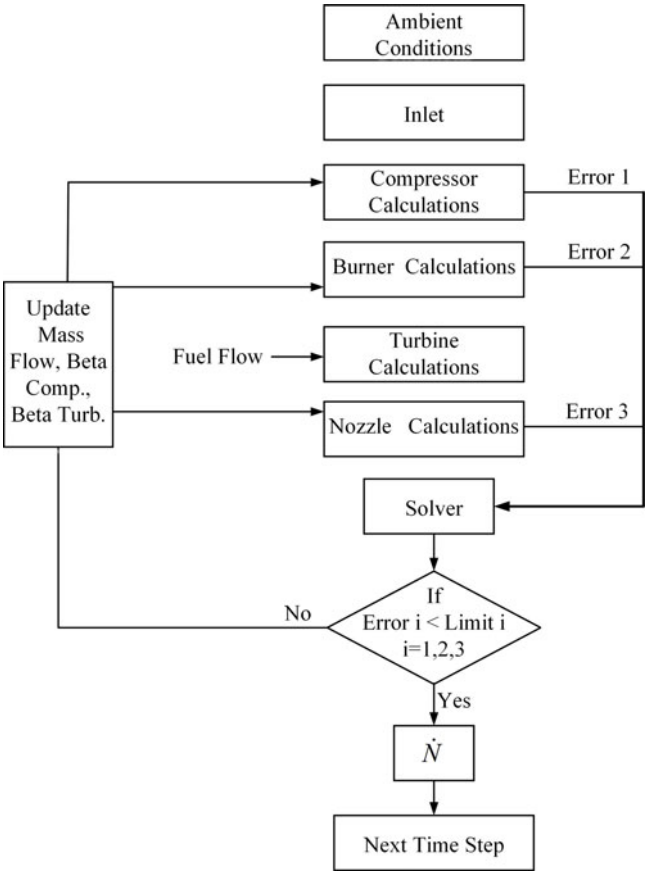


Figure 2. *Iterative procedure for engine thermodynamic modeling.*

where $\dot{N}$ is the shaft angular acceleration, $\Delta\tau$ represents the difference between the torque generated by the turbine and the torque demanded by the compressor, and J is the moment of inertia of the rotor. In order to obtain the thermodynamic model by matrix iteration technique, a number of engine parameters are guessed and the same number of errors are defined. For this objective, in this study, inlet air mass flow, beta values for the compressor and turbine are estimated and the errors related to mass conservation in the compressor, turbine and nozzle are considered. The guesses are updated at each iteration through a numerical procedure until the errors are less than a pre-defined value. The numerical process is generally performed using the iterative Newton–Raphson procedure [25]. Figure 2 shows the iterative process of solving the equations to achieve the transient model.

In order to show the validity of the modeling, according to Figs. 3 and 4, two important outputs of the engine (i.e., the thrust value and fuel flow) in terms of relative spool speed, have been compared with the engine test data. The maximum mismatch error for thrust is 3%, and for fuel consumption is 6%. Therefore, the obtained thermodynamic model has sufficient validity for performance analysis and controller design.

Because there is no explicit nonlinear dynamic equation for gas turbine engines, the nonlinear thermodynamic model is linearised around an operating point through identification techniques for the purpose of controller design. The linear model of the system with integrated input is expressed as

$$\begin{aligned} \dot{x} &= ax + bu \\ \dot{u} &= u_r \\ y_i &= c_i x + d_i u \end{aligned} \tag{6}$$

https://doi.org/10.1017/aer.2025.10051 Published online by Cambridge University Press

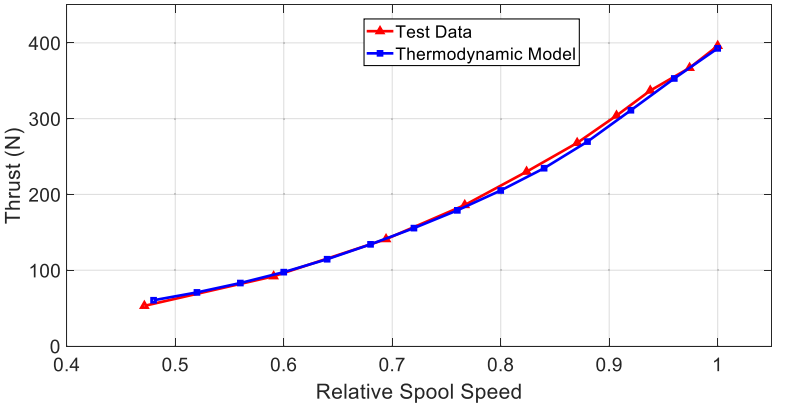


Figure 3. *Engine thrust versus relative spool speed.*

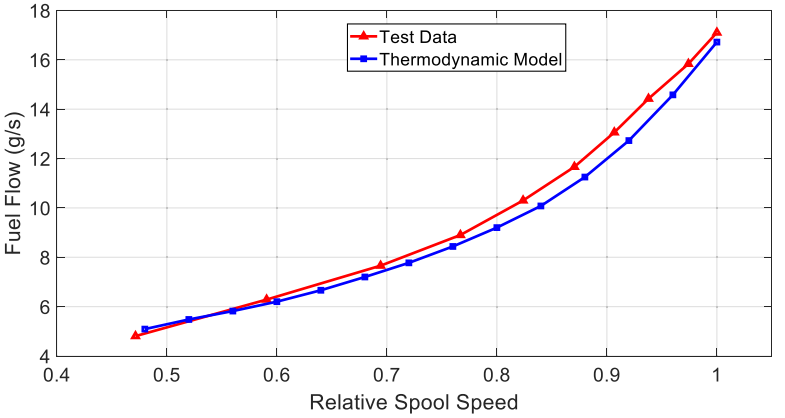


Figure 4. *Engine fuel flow versus relative spool speed.*

where $x = \Delta N$ is the state variable (i.e., engine speed increment) in rpm, $u = \Delta W_f$ is the control input (i.e., fuel flow increment) in kilograms per second (kg/s), and y_i are increments of the outputs.

3.0 Control strategy

The engine controller must provide the desired thrust and at the same time protect the limits of turbine temperature, maximum engine speed, compressor surge and combustion chamber blow-out. To achieve this objective, a selective control strategy [29, 30] has been taken into account. The structure of the proposed controller is illustrated in Fig. 5. Considering that engine thrust cannot be measured in flight conditions [31], therefore, a control loop is considered for engine spool speed as thrust representative. The relationship between thrust and engine speed is non-linear, and based on a lookup table, the thrust command is converted to its equivalent spool speed. This control loop should be designed in such a way that the response of the controller is without overshoot so that while providing the desired speed command, the engine speed does not exceed the maximum allowed value. As the engine speed increases, it's crucial that the temperature of the turbine remains within the acceptable range to prevent damage to the turbine blades. Measuring the turbine inlet temperature (TIT) directly is challenging due to its extreme heat. Consequently, to avoid exceeding TIT limit, it is managed indirectly through the regulation of the engine EGT. Therefore, an EGT control loop is included in the controller structure and its output is compared with the output of the previous loop and the minimum value is selected. A significant challenge

https://doi.org/10.1017/aer.2025.10051 Published online by Cambridge University Press

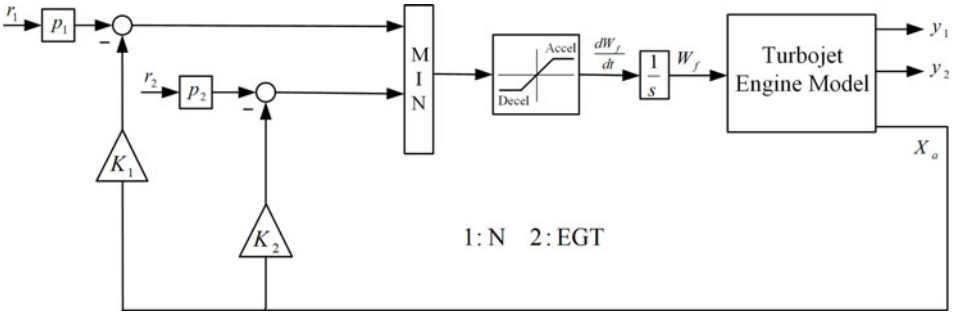


Figure 5. *The structure of the proposed controller.*

in engine control is the prevention of the dangerous compressor surge phenomenon. Since the risk of compressor surge increases during the engine's rapid acceleration, restricting the engine's acceleration can greatly minimise the probability of this occurrence. Limiting the acceleration of the engine can be achieved by limiting the fuel flow rate, therefore, by considering the output of the speed control loop and the EGT control loop as the fuel flow rate, and by using the upper saturation limit for the fuel flow rate, it is possible to prevent rapid acceleration and compressor surge [32, 33]. Another important challenge of the engine is the possibility of lean blow-out in the conditions of instantaneous throttle reduction. When the throttle is reduced abruptly, the fuel supplied by the power level angle (PLA) control loop is also immediately decreased. This leads to a significant drop in the fuel-to-air ratio and raises the risk of combustion chamber blow-out. To reduce this risk, the engine's deceleration is controlled. In this circumstance, a lower saturation limit for the fuel flow rate is considered to prevent the instantaneous reduction of the fuel flow and the combustion chamber blow-out. The output of the saturation function after passing through an integrator determines the amount of engine fuel. State feedback regulators are used to control engine speed and EGT temperature in the proposed controller structure.

In summary, it can be stated that the engine controller is responsible for meeting the required spool speed demand, which represents the thrust value, while also ensuring that the following variables remain within their limits during both steady-state and transient conditions:

$$\begin{cases} \Delta EGT\ (y_2 \le r_2) \\ \dfrac{dW_f}{dt}\ (u_{r\min} \le u_r \le u_{r\max}) \end{cases} \tag{7}$$

To formulate state feedback regulators, the linear system (1) can be expressed in the following augmented representation:

$$\begin{gathered} \dot{X} = AX + Bu_r \quad y_i = C_i X \\ A = \begin{bmatrix} a & b \\ 0 & 0 \end{bmatrix} B = \begin{bmatrix} 0 \\ 1 \end{bmatrix} C_i = \begin{bmatrix} c_i & d_i \end{bmatrix} \end{gathered} \tag{8}$$

where $X = \begin{bmatrix} x & u \end{bmatrix}^T$ is the augmented state vector. State feedback control law for each individual control loop is regarded as follows:

$$u_{ri} = -K_i X + p_i r_i \tag{9}$$

where feedback gain K_i is established employing state feedback methods to ensure that $A - BK_i$ remains stable, while each control loop exhibits satisfactory performance without any overshoot. The constant parameters of r_i, for $i = 1, 2$ consist of the setpoint for the main output and the limit value for the restricted output, both of which are determined based on the reference command and the characteristics of the system. The p_i gains are constant reference prefilter gains aimed at ensuring that $y_i = C_i X = r_i$ in steady-

https://doi.org/10.1017/aer.2025.10051 Published online by Cambridge University Press

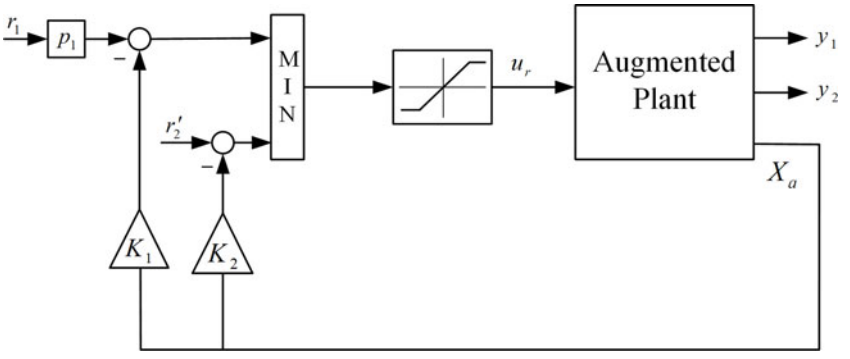


Figure 6. *Reconfiguration of the controller.*

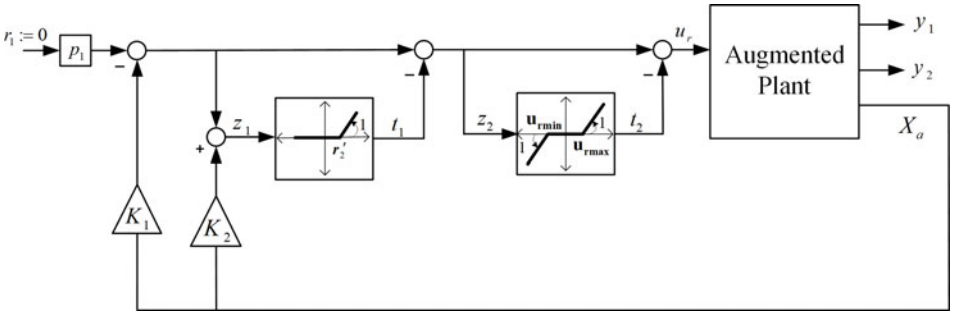


Figure 7. *New depiction of the controller.*

state condition. They are established based on the following relationship.

$$p_i = [-C(A - BK_i)^{-1}B]^{-1} \tag{10}$$

The following section presents a methodology for analysing the stability of the proposed control system.

4.0 Stability investigation

To investigate the stability of the designed controller depicted in Fig. 5, the controller's architecture is converted into the standard configuration of *Lure's system* [34]. To achieve this, the initial step involves reconfiguring the plant, as illustrated in Fig. 6, resulting in its transformation into an augmented form. In the new configuration, $r_2' = r_2 p_2$. After that, according to Fig. 7, the Min selector and saturation function are replaced with their nonlinear equivalents [35]. In order to use the techniques of *Lure's problem* [34], the dynamics between the outputs t_i and inputs z_i of the nonlinear memory-less functions are extracted. Hence, using Fig. 7, we have

$$\begin{cases} z_1 = -K_1X + K_2X = (K_2 - K_1)X \\ z_2 = -K_1X - t_1 \end{cases} \tag{11}$$

The relationship between $X = [x \;\; u]^T$ and u_r can be determined from the transfer functions of the augmented plant, which is expressed as follows:

$$G(s) = [\, G_1(s) \quad G_2(s)\,]^T = \left[\frac{x(s)}{u_r(s)} \quad \frac{u(s)}{u_r(s)} \right]^T \tag{12}$$

control input rate is established from Fig. 7 based on the following equation:

$$u_r = -K_1X - t_1 - t_2 \tag{13}$$

https://doi.org/10.1017/aer.2025.10051 Published online by Cambridge University Press

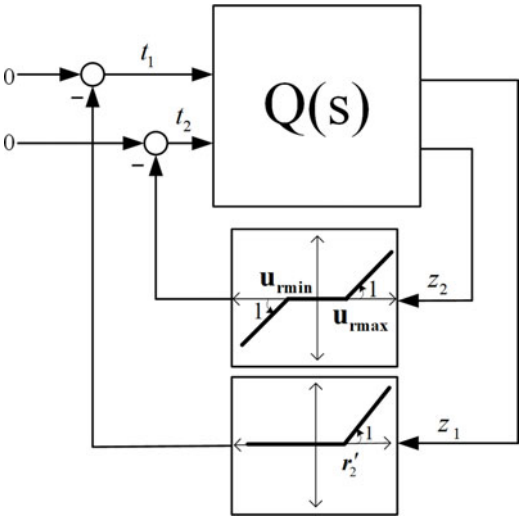


Figure 8. *Closed-loop system arranged in a standard configuration.*

by applying Equations (12) and (13), $X = [x \quad u]^T$and u_r are derived according to the values of t_i. Substituting X into Equation (11) reveals the relationship between t_i and z_i. Consequently, the control system illustrated in Fig. 7 can be represented as shown in Fig. 8, where matrix $Q(s)$ expresses the dynamic relationship,

$$Q(s) = \frac{\begin{bmatrix} (K_2 - K_1)G & (K_2 - K_1)G \\ 1 & -K_1 G \end{bmatrix}}{K_1 G + 1} \tag{14}$$

K_i are state feedback gains and G is the vector of transfer functions (12).

The updated configuration, referred to as Lure's system, incorporates a dynamic multivariate block along with static nonlinearities in the feedback loop. Based on the multivariate circle criterion [34], if $Q(s)$ represents a square and proper transfer function matrix with the following minimal realisation,

$$\begin{cases} \dot{X} = \hat{A}X + \hat{B}T \\ Z = \hat{C}X + \hat{D}T \end{cases} \tag{15}$$

where $T = -\Lambda(Z)$, and $\Lambda(\cdot)$ is a vector containing static nonlinearities which are locally Lipschitz in Z and this vector satisfies the sector condition defined by real diagonal matrices Ω_1 and Ω_2 (i.e., $[\Lambda(Z) - \Omega_1 Z]^T [\Lambda(Z) - \Omega_2 Z] \leq 0$), then the closed-loop system is globally asymptotically stable (or absolutely stable) around the equilibrium point $X = 0$, if $[I + \Omega_2 Q][I + \Omega_1 Q]^{-1}$ is strictly positive real. According to the static non-linear functions depicted in Fig. 8, matrix Ω_1 is defined as a zero matrix. Consequently, to ensure asymptotic stability, it suffices for matrix $[I + \Omega_2 Q]$ to be strictly positive real. To check the strictly positive real condition, the following lemma is taken into account [36]:

Lemma [36]: Let N(s) be a transfer function matrix with minimal realisation matrices (E, F, H, J), then the following statements are equivalent:

(1) E is a Hurwitz matrix and N(s) is strongly positive real

(2) $J + J^T > 0$ and there exist positive definite matrices P and R such that

$$E^T P + PE + (H - F^T P)^T (J + J^T)^{-1} (H - F^T P) + R = 0$$

It's important to emphasise that strongly positive real implies strictly positive real [36].

https://doi.org/10.1017/aer.2025.10051 Published online by Cambridge University Press

Utilising the minimum realisation of $Q(s)$, we find that the minimal realisation matrices of $[I + \Omega_2 Q]$ are $(\hat{A}, \hat{B}, \Omega_2\hat{C}, I + \Omega_2\hat{D})$. Now, according to the lemma statements, if matrix $\hat{A}$ is Hurwitz and $2I + \Omega_2\hat{D} + \hat{D}^T\Omega_2$ is positive definite, and if there exist positive definite matrices P and R such that fulfill the Riccati Equation (16), then $[I + \Omega_2 Q]$ is strictly positive real and the multivariate circle condition is satisfied:

$$\hat{A}^T P + P\hat{A} + [\Omega_2\hat{C} - \hat{B}^T P]^T[2I + \Omega_2\hat{D} + \hat{D}^T\Omega_2]^{-1}[\Omega_2\hat{C} - \hat{B}^T P] + R = 0 \tag{16}$$

Consequently, the control system's asymptotic stability around the origin $X = 0$ is assured, and $V = X^T PX$ is derived as a Lyapunov function for the closed-loop system [36]. The asymptotic stability of the designed controller is investigated in the following section.

5.0 Results and discussion

To design the controller, assess its stability, and evaluate its performance, the nonlinear model has been linearised around an operating point (altitude = 0, Mach = 0 and $W_f = 15.5g/s$). The parameters of the linear model include:

$$\begin{aligned} a &= -2.034, \quad b = 3.337 \times 10^6 \\ \Delta N : c &= [1 \quad 0], \quad d = 0 \\ \Delta EGT : c &= [0.02153 \quad 0], \quad d = 0 \end{aligned} \tag{17}$$

Linear model (6) with the aforementioned parameters is both controllable and observable. State feedback regulators for the engine speed control loop and EGT are designed using pole placement technique. Each loop's regulator is designed to ensure that the isolated loop remains stable while providing satisfactory performance. Consequently, the control gains are determined as follows:

$$\begin{aligned} K_1 &= [5.691e-7 \quad 4.966], \\ K_2 &= [2.047e-7 \quad 3.966] \end{aligned} \tag{18}$$

prefilter gains p_i are also obtained from Equation (10). The limit values of the restricted variables for linear system are taken into account as follows:

$$r_2 = 115K, u_{r\max} = 0.02kg/s^2, \quad u_{r\min} = -0.02kg/s^2 \tag{19}$$

For the stability analysis of the closed-loop system, the transfer function vector G is determined as:

$$G(s) = \left[\frac{3.337e6}{s^2 + 2.034s} \quad \frac{1}{s}\right]^T \tag{20}$$

The equivalent linear system $Q(s)$ is defined in accordance with Equation (16) as follows:

$$Q(s) = \frac{\begin{bmatrix} -\mathrm{s} - 3.25 & -\mathrm{s} - 3.25 \\ s^2 + 2.034s & -4.966\mathrm{s} - 12 \end{bmatrix}}{s^2 + 7s + 12} \tag{21}$$

A minimal state space realisation of $Q(s)$ is determined:

$$\hat{A} = \begin{bmatrix} -3.3853 & 7.0337 \\ 00337 & -3.6147 \end{bmatrix}$$

$$\hat{B} = \begin{bmatrix} -0.9583 & -0.9583 \\ 1.1419 & 1.1419 \end{bmatrix}$$

https://doi.org/10.1017/aer.2025.10051 Published online by Cambridge University Press

Table 2. *The limits of the limited variables in nonlinear simulation*

Limited variable	**Limit value**
Maximum exhaust gas temperature (K)	1123
Maximum fuel flow rate (g/s^2)	20
Minimum fuel flow rate (g/s^2)	−20

$$\hat{C} = \begin{bmatrix} 0.0138 & -0.8642 \\ 0.6001 & -3.8454 \end{bmatrix}$$

$$\hat{D} = \begin{bmatrix} 0 & 0 \\ 1 & 0 \end{bmatrix} \tag{22}$$

The matrices Ω_1 and Ω_2, which define the sectors, are established as follows:

$$\Omega_1 = 0 \times I_2, \quad \Omega_2 = 0.97 \times I_2 \tag{23}$$

where I_2 is the 2×2 identity matrix. Based on the conditions obtained for the stability analysis, $\hat{A}$is Hurwitz and $2I + \Omega_2\hat{D} + \hat{D}^T\Omega_2$is positive definite. The Riccati Equation (6) can be formulated as a Linear Matrix Inequality (LMI) feasibility problem by utilising the Schur complement lemma [37]. Therefore, the positive definite matrix P needs to satisfy the following inequality:

$$\begin{bmatrix} \hat{A}^TP + P\hat{A} & P\hat{B} - \hat{C}^T\Omega_2 \\ \hat{B}^TP - \Omega_2\hat{C} & -2I - \Omega_2\hat{D} - \hat{D}^T\Omega_2 \end{bmatrix} < 0 \tag{24}$$

By addressing this feasibility problem, a positive definite matrix P is derived as follows:

$$P = \begin{bmatrix} 0.3253 & -0.7470 \\ -0.7470 & 2.8457 \end{bmatrix} \tag{25}$$

Consequently, the asymptotic stability of the control system around $X = 0$ is assured, and the Lyapunov function $V = X^TPX$ for the closed-loop system is established.

To assess the effectiveness of the proposed control structure, its performance is compared to a PI controller. The PI controller controls the engine spool speed as thrust representative, and has been developed based on the spool speed transfer function at the specified operating point. This controller has an efficient manner in tracking the desired input. For instance, its response to the step command is almost overshoot-free (overshoot is less than 0.4%) and its rise time is 0.87 s. The gains of the designed PI controller are:

$$K_p = 6.3 \times 10^{-7}, \quad K_i = 1.5 \times 10^{-6} \tag{26}$$

The limit values of the constrained variables for nonlinear simulation are presented in Table 2. The PLA degree is proportional to the thrust value, but it has a non-linear relationship with spool speed. As shown in Fig. 9, a comprehensive command for the PLA degree around the operating point is defined in the International Standard Atmosphere (ISA) and zero Mach and standard sea level (SLS) altitude conditions. PLA degree starts from 92% and varies between 75% and 100%. The system response is not necessarily satisfactory for simulation at lower PLA degree as well as at other Mach numbers and altitudes. Figure 10 shows the response of the controllers in tracking the desired thrust. The response of the PI controller is faster than the selector controller, but it has overshoot and undershoot in some places. As mentioned before, considering that the thrust value cannot be measured in flight conditions, this parameter is indirectly controlled through the engine speed. In Fig. 11, the process of following the desired spool speed using two controllers is shown. The response speed of the PI controller is slightly higher than that of the switching controller, but in some places, this controller has a limited overshoot and undershoot. Figure 12 illustrates the variations in the engine exhaust gas temperature for both controllers. The PI controller significantly surpasses the specified limit. This is because the PI controller just controls

https://doi.org/10.1017/aer.2025.10051 Published online by Cambridge University Press

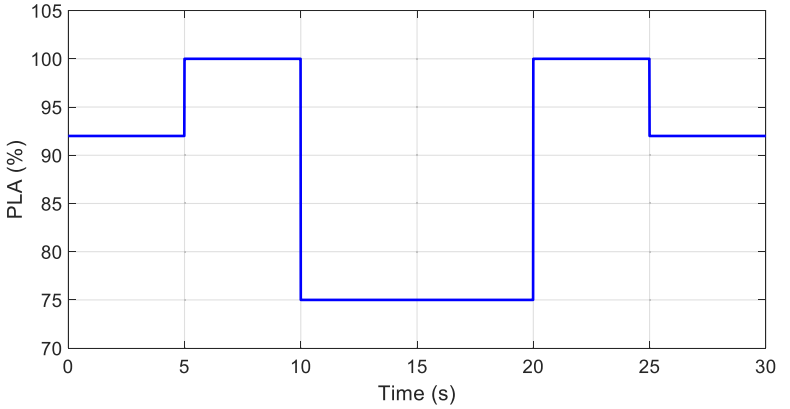


Figure 9. *Throttle command.*

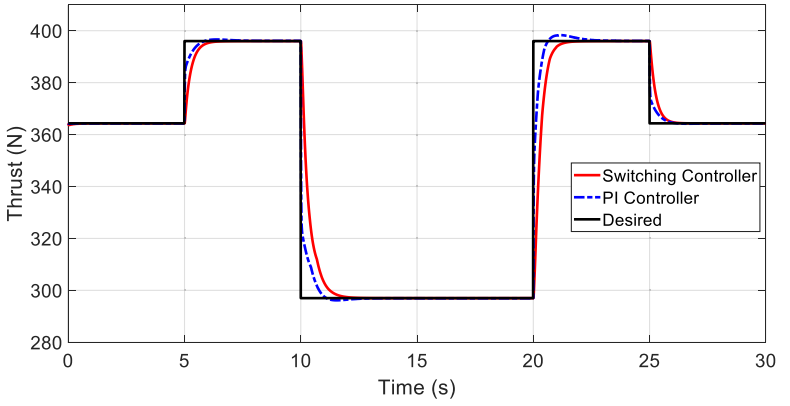


Figure 10. *Engine thrust response.*

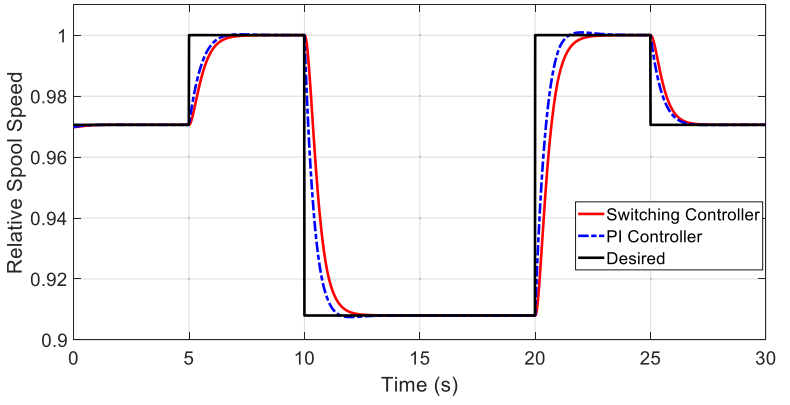


Figure 11. *Spool speed response.*

engine speed as the thrust representative it does not have any feedback from the limit violation of other engine outputs. Consequently, its efficacy in safeguarding the EGT limit is unacceptable. In Fig. 13, the surge margin of the compressor is indicated for both controllers. According to this figure, due to the presence of fuel flow rate saturation in the structure of the selector controller, this controller has a higher surge margin.

https://doi.org/10.1017/aer.2025.10051 Published online by Cambridge University Press

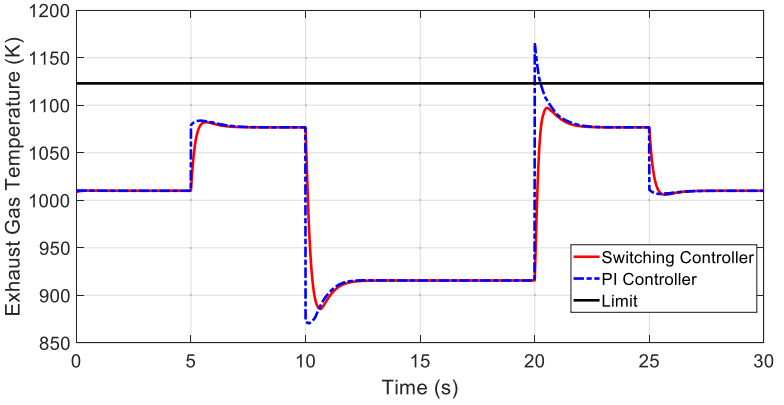


Figure 12. *Exit gas temperature response.*

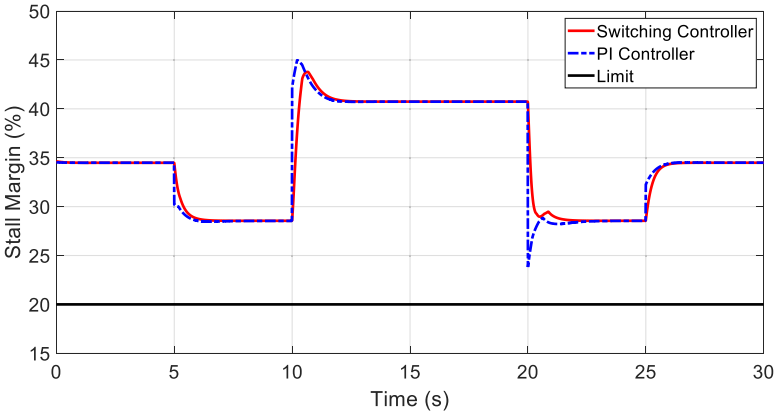


Figure 13. *Surge margin.*

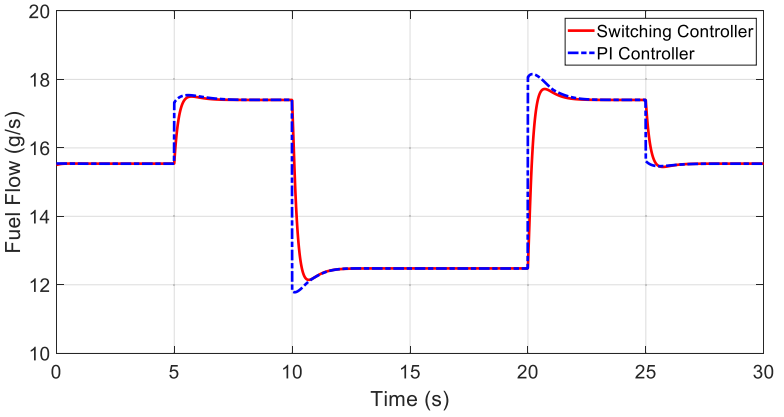


Figure 14. *Fuel consumption.*

Figure 14 illustrates the variations in fuel consumption by two controllers to achieve the desired thrust. The findings indicate that while the PI controller effectively provides engine thrust quickly and with precision, it also leads to issues such as overshoot and undershoot, as well as violations of limits for some critical outputs. These problems can diminish efficiency, shorten engine life and, in some cases, result in engine failure. On the other hand, the selector controller not only manages thrust control but also

https://doi.org/10.1017/aer.2025.10051 Published online by Cambridge University Press

safeguards the engine's structural and operational constraints, ensuring a precise and secure response. It should be noted that, although the proposed controller has been designed around an operating point, the simulation has been done on a nonlinear model with the presence of uncertainty and model mismatch. This shows the accurate and robust operation of the designed controller. To apply the proposed method for engine control in a full flight envelope, the flight envelope must be divided into multiple regions and a controller with the proposed structure must be designed for each region. Then, the controller gains are adjusted based on the gain scheduling method.

5.0 Conclusion

Most of the presented methods for controlling small turbojet engines are based on classical control methods and have only focused on engine thrust control and have not provided an effective manner to manage engine limitations in different operational conditions. The main reason for this issue is the limited number of sensors and actuators in this category of engines. These engines typically have a simple structure and a small number of elements, and only the engine spool speed and the temperature of the exhaust gas are measured by sensors. In the present research, a control algorithm including an engine speed control loop as thrust representative and a turbine temperature control loop was defined using the state feedback technique. In order to maintain the limitations of the engine related to the compressor surge margin and combustion chamber blow-out in the transient regime, a saturation function was considered for the engine fuel flow rate. Then an effective solution was presented to check the stability of the closed loop system. The performance evaluation of the proposed control method to control a small turbojet engine in ISA and SLS conditions showed that the requested thrust is provided accurately and without overshoot and the constraints governing the engine variables are protected. To use this method to control the engine for full flight envelope, the flight envelope must be divided into several regions. Then, for each region, a minimum selector controller is designed and its stability analysis is carried out. After that, using the gain scheduling method, the controller gains are adjusted. The presented procedure is applicable for all engines that have similar conditions.

Competing interests. The author declares none.

References

[1] Catana, R.M., Cican, G. and Badea, G.P. Thermodynamic analysis and performance evaluation of microjet engines in gas turbine education, *J. Appl. Sci.*, 2024, **14**, p 6754, doi: 10.3390/app14156754

[2] Erario, M.L., De Giorgi, M.G. and Przysowa, R. Model-based dynamic performance simulation of a microturbine using flight test data, *Aerospace*, 2022, **9**, (2), p 60, doi: 10.3390/aerospace9020060

[3] Gaitanis, A., Contino, F. and Paepe, W.D. Real time micro gas turbines performance assessment tool: comprehensive transient behavior prediction with computationally effective techniques, *J. Eng. Gas. Turbines Power*, 2023, **145**, (3), p 031006, doi: 10.1115/1.4055785

[4] Many, M., Weber, M., Oberndorfer, S., Koeberle, S.J., Hosseini, B. and Hornung, M. System identification of a turbojet engine using multi-sine inputs in ground testing, Deutscher Luft- und Raumfahrtkongress, 2012. doi: 10.25967/550281

[5] Momin, A.J.A., Nava, G., L'Erario, G., Mohamed, H.A.O., Bergonti, F., Vanteddu, P.R., Braghin, F. and Pucci, D. Nonlinear model identification and observer design for thrust estimation of small-scale turbojet engines, 2022 International Conference on Robotics and Automation (ICRA), Philadelphia, PA, USA, doi: 10.1109/ICRA46639.2022.9812283

[6] Metin, E.Y. and Aygün, H. Energy and power aspects of an experimental target drone engine at non-linear controller loads, *Energy*, 2019, **185**, pp 981–993. doi: 10.1016/j.energy.2019.07.103

[7] Aygun, H., Dursun, O.O., Dönmez, K., Sahin, O. and Toraman, S. Prediction of performance characteristics of an experimental micro turbojet engine using machine learning approaches, *Energy*, 2024, **313**, p 133997. doi: 10.1016/j.energy.2024.133997

[8] Banazadeh, A., Gol, H.A. and Ramazani, H. PID controller design for micro gas turbines using experimental frequency-response data and a linear identification technique, *Int. J. Adv. Mechatron. Syst.*, 2013, **5**, (6), pp 353–364, doi: 10.1504/IJAMECHS.2013.060016

[9] Andoga, R., Főző, L., Judičák, J., Bréda, R., Szabo, S., Rozenberg, R. and Džunda, M. Intelligent situational control of small turbojet engines, *Int. J. Aerospace Eng.*, 2018, doi: 10.1155/2018/8328792

https://doi.org/10.1017/aer.2025.10051 Published online by Cambridge University Press

[10] Beneda, K. and Derbel, K. Design of two-degree-of-freedom turbofan-power-ratio control system for micro turbojet engine, 2019 IEEE 17th World Symposium on Applied Machine Intelligence and Informatics (SAMI), Herlany, Slovakia, doi: 10.1109/SAMI.2019.8782788
[11] Derbel, K. and Beneda, K. Sliding mode control for micro turbojet engine using turbofan power ratio as control law, *Energies*, 2020, **13**, (18), p 4841, doi: 10.3390/en13184841
[12] Tang, W., Wang, L., Gu, J. and Gu, Y. Single neural adaptive PID control for small UAV micro-turbojet engine, *Sensors*, 2020, **20**, (2), p 345, doi: 10.3390/s20020345
[13] Shehata, A.M., Khalil, M.K. and Ashry, M.M. Controller design for micro turbojet engine, 2020 12th International Conference on Electrical Engineering (ICEENG), pp 436–440, doi: 10.1109/ICEENG45378.2020.9171762
[14] Shehata, A.M., Khalil, M.K. and Ashry, M.M. Adaptive fuzzy PID controller applied to micro turbojet engine, *J. Phys.: Conf. Ser.*, 2021, **2128**, (1), p 012030, doi: 10.1088/1742-6596/2128/1/012030
[15] Gao, Q., Li, J. and Zhang, Y. Self-tuning speed and flow control of micro turbojet engines based on an improved evolutionary strategy, *Automatika*, 2024, **65**, (3), pp 1154–1162, doi: 10.1080/00051144.2024.2349869
[16] Wang, N., Xu, J. and Li, Z. The active disturbance rejection control method for small-scale turbojet engine, *J. Phys. Conf. Ser.*, 2024, **2764**, p 012065, doi: 10.1088/1742-6596/2764/1/012065
[17] Jafari, S. and Nikolaidis, T. Turbojet engine industrial Min–Max controller performance improvement using fuzzy norms, *Electronics*, 2018, **7**, (314), doi: 10.3390/electronics7110314
[18] Garg, S. *Aircraft Turbine Engine Control Research at NASA Glenn Research Center, NASA/TM-2013-217821*, Glenn Research Center, 2013, Cleveland, Ohio.
[19] Imani, A. and Montazeri-Gh, M. Improvement of min-max limit protection in aircraft engine control: an lmi approach, *J. Aerospace Sci. Technol.*, 2017, **68**, pp 214–222, doi: 10.1016/j.ast.2017.05.017
[20] Authié, P. Multi-model structured h-infinity design of a robust and aggressive turbofan jet engine controller, *Lett. Dyn. Syst. Control*, 2022, **2**, (2), p 021008, doi: 10.1115/1.4052916
[21] Richter, H. A multi-regulator sliding mode control strategy for output constrained systems, *Automatica*, 2011, **47**, (10), pp 2251–2259, doi: 10.1016/j.automatica.2011.08.003
[22] Imani, A. and Montazeri-Gh, M. A Min–Max multiregulator system with stability analysis for aeroengine propulsion control, *ISA Trans.*, 2019, **85**, pp 84–96, doi: 10.1016/j.isatra.2018.10.035
[23] AMT. Titan gas turbine manual, AMT Netherlands, 2014.
[24] Savvaris, A., Buonanno, A., Jamil, R. and Tsourdos, A. Design and development of the DEMON UAV fluidic flight control system, 2013 In AIAA Infotech@ Aerospace (I@ A) Conference, p 4820. doi: 10.2514/6.2013-4820
[25] Walsh, P.P. and Fletcher, P. Gas Turbine Performance, John Wiley & Sons, 2004, doi: 10.1002/9780470774533
[26] Lichtsinder, M. and Levy, Y. Jet engine model for control and real-time simulations, *J. Eng. Gas Turb. Power*, 2006, **128**, (4), pp 745–753, doi: 10.1115/1.1915391
[27] Zinnecker, A., Chapman, J.W., Lavelle, T.M. and Litt, J.S. Development of a twin-spool turbofan engine simulation using the Toolbox for Modeling and Analysis of Thermodynamic Systems (T-MATS), 50th AIAA/ASME/SAE/ASEE Joint Propulsion Conference, Cleveland, OH, 2014, doi: 10.2514/6.2014-3930
[28] Chung, G.Y., Prasad, J., Dhingra, M. and Meisner, R. Real time analytical linearization of turbofan engine model, *J. Eng. Gas Turb. Power*, 2014, **136**, (1), p 011201, doi: 10.1115/1.4025310
[29] Cai, C., Wang, Y., Chen, H., Zheng, Q. and Zhang, H. Full-envelope acceleration control method of turbofan engine based on variable geometry compound adjustment, *J. Aerospace Sci. Technol.*, 2022, **128**, p 107748, doi: 10.1016/j.ast.2022.107748
[30] Eslami, M. and Banazadeh, A., Control performance enhancement of gas turbines in the minimum command selection strategy, *ISA Trans.*, 2021, **112**, pp 186–198, doi: 10.1016/j.isatra.2020.12.003
[31] Singh, R., Maity, A. and Nataraj, P.S.V. Dynamic modeling and robust nonlinear control of a laboratory gas turbine engine, *J. Aerospace Sci. Technol.*, 2022, **126**, p 107586, doi: 10.1016/j.ast.2022.107586
[32] DeCastro, J.A., Litt, J.S. and Frederick, D.K. A modular aero-propulsion system simulation of a large commercial aircraft engine, NASA/TM2008-215303, Glenn Research Center, Cleveland, Ohio, 2008.
[33] Litt, J.S., Frederick, D.K. and Guo, T.H. The case for intelligent propulsion control for fast engine response, NASA/TM2009-215668, Glenn Research Center, Cleveland, Ohio, 2009.
[34] Khalil, H.K. Nonlinear Control, Global Ed, Pearson Education, 2015.
[35] Imani, A. and Montazeri-Gh, M. A Multi-loop switching controller for aircraft gas turbine engine with stability proof, *Int. J. Control Autom.*, 2019, **17**, (6), pp 1359–1368, doi: 10.1007/s12555-018-0803-5
[36] Haddad, W.M. and Bernstien, D.S. Explicit construction of quadratic lyapunov functions for the small gain, positivity, circle, and popov theorems and their application to robust stability. Part I: continuous-time theory, *Int. J. Robust Nonlinear*, 1993, **3**, (4), pp 313–339, doi: 10.1002/rnc.4590030403
[37] Geromel, J.C. *Differential Linear Matrix Inequalities: In Sampled-Data Systems Filtering and Control*, Springer, 2023, doi: 10.1007/978-3-031-29754-0

Cite this article: Imani A. (2025). A minimum selection strategy for control of small-scale turbojet engines. *The Aeronautical Journal*, **129**, 3467–3483. https://doi.org/10.1017/aer.2025.10051

https://doi.org/10.1017/aer.2025.10051 Published online by Cambridge University Press